Preparation of Sunflower Straw Cellulose Nanofibers/ Poly(lactic acid)/ Poly(butylene adipate-co-terephthalate) Composites by Co-precipitation and Hot-pressing

Yueru Wang,[a] Zhenyu Chen,[a] Ziming Zhao,[a] and Guichang Jiang [a,b,*]

Polylactic acid (PLA) is a rigid biopolymer, while poly(butylene adipate-co-terephthalate) (PBAT) is a flexible biodegradable polymer. To comprehensively enhance the mechanical properties of PLA/PBAT composites, sunflower straw cellulose nanofibers (SSCNFs) were isolated from sunflower straw (SS) *via* TEMPO oxidation treatments and used as reinforcement. Using a PLA/PBAT blend (60:40 by mass) as the matrix, SSCNFs-reinforced PLA/PBAT composites were prepared using a co-precipitation and hot-pressing method. The morphology and structure of the SSCNFs were characterized by Fourier transform infrared spectroscopy (FTIR), scanning electron microscopy (SEM), and nanoparticle size and zeta potential analysis. The mechanical and thermal properties of the composites were tested. The tensile and flexural properties of the composites were improved with increasing SSCNFs content. When the SSCNF content was 16 wt%, the composites reached a tensile strength of 20.06 ± 0.61 MPa (an 11.69% enhancement), a tensile modulus of 732.57 ± 42.72 MPa (a 56.64% enhancement), a flexural strength of 31.76 ± 0.54 MPa (a 20.21% enhancement), and a flexural modulus of 2030.42 ± 36.37 MPa (a 77.50% enhancement). Although thermal stability and water absorption were slightly decreased, UV shielding capacity and hydrophobicity were enhanced. The prepared composites exhibited well-balanced overall performance and potential for replacing traditional commercial polymers.

DOI: 10.15376/biores.21.2.2815-2831

Keywords: Sunflower straw cellulose nanofibers (SSCNFs); PLA; PBAT; Co-precipitation hot-pressing method; Composites

Contact information: a: Tianjin University of Science and Technology, Tianjin 300222, People's Republic of China; b: Dept of Chemistry, Tsinghua University, Beijing 100084, People's Republic of China;
** Corresponding author: gcj@tust.edu.cn*

INTRODUCTION

As an agricultural waste, sunflower straw (SS) often has been neglected or simply discarded in the past through methods such as burning or landfill disposal. These practices not only waste a valuable resource but also pose a risk of environmental pollution (Binici *et al*. 2020). However, with advancements in science and technology and a growing emphasis on resource recycling, the potential value of sunflower straw has been increasingly recognized and utilized (Dalmis 2023). Sunflower straw has a high cellulose content of approximately 41% (Xu *et al*. 2020), making it a suitable raw material for the preparation of nanocellulose.

Several researchers have explored methods to produce nanocellulose from sunflower straw. For instance, Fortunati *et al.* (2016) successfully prepared nanocellulose from sunflower straw using steam explosion. Yan *et al.* (2023) isolated nanocellulose with a length of approximately 2.0 μm and a width of approximately 26.3 nm from the pith of sunflower stems *via* TEMPO oxidation. Similarly, Ewulonu *et al.* (2019) produced lignocellulosic nanofibers from sunflower stalks using a combination of sulfuric acid hydrolysis, ball milling, and ultrasonication.

Polylactic acid (PLA) is a bio-based thermoplastic. However, it suffers from low toughness and poor heat resistance (Jamshidian *et al*. 2010). Additionally, due to the costs associated with production technology and raw materials, the price of PLA is typically higher than that of conventional petroleum-based plastics. Poly(butylene adipate-co-terephthalate) (PBAT) is another type of thermoplastic biodegradable polymer. Blending PBAT with other biodegradable materials, such as PLA or starch, can effectively modify its properties; for example, it can enhance toughness and reduce overall material costs. By blending PLA and PBAT, a composite material that combines the advantages of both polymers can be achieved. This synergy results in a material that exhibits the hardness and rigidity of PLA alongside the flexibility and high tensile strength of PBAT, thereby expanding its potential applications (Da Costa *et al*. 2023). Furthermore, the mechanical and thermal properties of PLA/PBAT blends can be further enhanced by incorporating nanomaterials or inorganic fillers (Taguet *et al*. 2014; Salzano de Luna and Filippone 2016). For instance, Deniz Sema Sarul *et al.* (2021) prepared cellulose nanocrystal (CNC)-reinforced PLA/PBAT blend nanocomposites using melt compounding with a twin-screw extruder. Similarly, Yan *et al.* (2020) fabricated nano-hydroxyapatite/PLA/PBAT/ microcrystalline cellulose (MCC) composites *via* a solution blending method. The role of the co-precipitation hot-pressing method in dispersing SSCNFs and establishing their interfacial compatibility with PLA/PBAT has not been systematically investigated.

SSCNFs, which are cellulose nanofibers extracted from sunflower straw through alkali and TEMPO oxidation, possess a high specific surface area, a high aspect ratio, and excellent mechanical properties. The hypothesis of this study is that the co-precipitation method promotes PLA/PBAT molecular chain extension and achieves composites with optimal properties at a specific SSCNFs content. Therefore, in this study, the sunflower straw cellulose nanofibers (SSCNFs) were prepared *via* the TEMPO oxidation method, while the PLA/PBAT composite matrix was fabricated using a co-precipitation method. The SSCNFs were then incorporated into the PLA/PBAT matrix at varying mass fractions. The SSCNFs/PLA/PBAT composites were subsequently consolidated using a hot-pressing technique.

The influence of different SSCNFs loadings on the properties of the PLA/PBAT composites was investigated to determine the optimal formulation. This approach successfully developed a novel biodegradable composite material exhibiting excellent mechanical properties, thermal stability, and degradability, with potential for broad applications in packaging, agriculture, and construction. Consequently, this study explores the application prospects of the combined co-precipitation and hot-pressing method for fabricating biodegradable composites, providing novel insights and methodologies for composite preparation. Furthermore, this work not only enhances the resource utilization of agricultural waste, mitigating its environmental impact, but also offers new material choices and technical support for the environmental protection industry, thereby contributing to its sustainable development.

EXPERIMENTAL

Materials

Sunflower straw was obtained from the Inner Mongolia Autonomous Region, China. Polylactic acid (PLA, grade 4043D) was supplied by Nature Works Co., Ltd. (USA). Poly(butylene adipate-co-terephthalate) (PBAT, grade TH801T) was supplied by Xinjiang Lanshan Tunhe Polyester Co., Ltd. (China). A chain extender, Joncryl® ADR-4468, was supplied by BASF SE (Germany). Dimethyl sulfoxide (DMSO), sodium hydroxide (NaOH), sodium hypochlorite (NaClO), 2,2,6,6-tetramethylpiperidine-1-oxyl (TEMPO), sodium bromide (NaBr), and absolute ethanol were purchased from Tianjin Fengchuan Chemical Reagent Technology Co., Ltd. (China). Sodium chlorite ($NaClO_2$) and glacial acetic acid were purchased from Shanghai Macklin Biochemical Co., Ltd. (China).

Methods

Preparation of SSCNFs

The sunflower straw was crushed into powder and passed through a 60-mesh standard sieve to obtain sunflower straw powder. First, the sunflower straw powder was bleached at 80 °C for 2 h in a sodium chlorite solution with a mass concentration of 3% (pH 4 to 5). After that, it was placed in a NaOH solution with a mass concentration of 4% and reacted at 80 °C for 2 h, washed to neutral after the reaction, and freeze-dried to obtain sunflower straw microcrystalline cellulose (SSMCC). A total of 1 g of SSMCC was dissolved in 100 mL of deionized water and sonicated in a cold-water bath at 500 W power for 2 h. After that, 0.01 g TEMPO and 0.1 g NaBr were added, and the mass molar concentration of 15 mmol/g sodium hypochlorite solution was slowly added dropwise. The pH of the reaction system was maintained at about 10.5 with NaOH at a concentration of 0.5 mol/L. After 2 h of reaction, 10 mL of absolute ethanol was added to stop the reaction, the mixed solution containing SSMCC was washed to neutral and dispersed in 100 mL of deionized water. Then, SSCNFs were obtained by ultrasonication at a power of 1200 W for 30 min in an ice water bath and freeze-dried into powder for later use.

Co-precipitation method preparation of PLA/PBAT composite powder

The PLA granules (60 g), PBAT granules (40 g), and BASF chain extender ADR (2.5 g) were dissolved in 1 L of DMSO. The solution was heated in a water bath at 90 °C for 1.5 h with continuous stirring. Upon completion of the reaction, the homogeneous blend solution was dripped into an excess of ice-cold deionized water at a controlled rate to induce co-precipitation *via* complete solvent exchange (DMSO to water). The resulting white precipitate was then collected by filtration, thoroughly dried (70 °C, 24 h), and ground into a fine powder for subsequent use.

Preparation of SSCNFs/PLA/PBAT composites

The SSCNFs powder prepared in the above step was thoroughly blended with the PLA/PBAT composite powder according to the mass ratios specified in Table 1. A predetermined amount of the blended powder was then evenly spread into a dumbbell-shaped hot-pressing mold. The sample was hot-pressed at 160 °C under a pressure of 2 tons (t) for 8 min. Subsequently, the mold was cooled to room temperature to solidify the composite, yielding a dumbbell-shaped SSCNFs/PLA/PBAT composite specimen with final dimensions of 150 × 10 × 1 mm^3.

Table 1. Ratio of SSCNFs Powder to PLA/PBAT Composite Powder

Sample Name	Quality of SSCNFs (g)	Quality of PLA/PBAT (g)
0% SSCNFs	0	100
4% SSCNFs	4	96
8% SSCNFs	8	92
12% SSCNFs	12	88
16% SSCNFs	16	84
20% SSCNFs	20	80

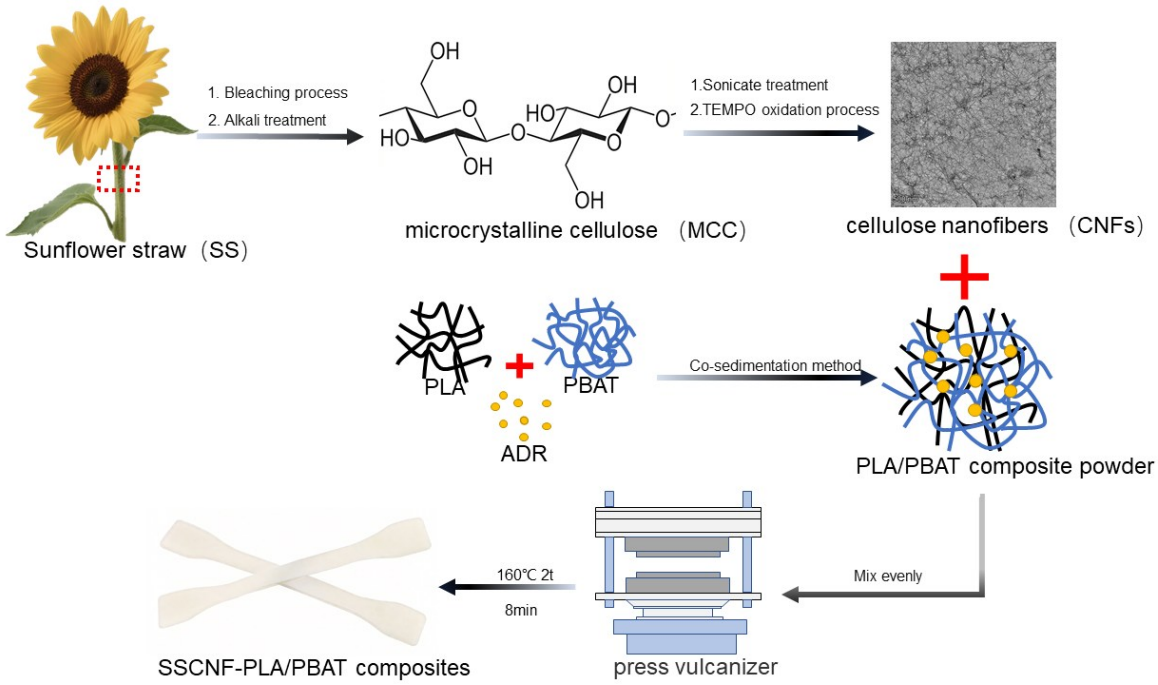

Fig. 1. Schematic illustration of the fabrication of SSCNFs/PLA/PBAT composites

Characterization

Nanoparticle size and zeta potential analysis

The SSCNFs suspension was diluted 100-fold using deionized water as the dispersant. For particle size analysis, the diluted sample was transferred into a cuvette, filling it to approximately one-third of its height. The instrument parameters were set as follows: a refractive index of 1.5, an equilibrium temperature of 25 °C, and an equilibration time of 25 s. The reported result represents the average of three independent measurements. For zeta potential measurement, the sample was loaded into a dedicated electrophoretic cell. The same sample parameters (refractive index, *etc.*) as those used for the particle size analysis were applied.

Fourier transform infrared spectroscopy (FTIR)

The SSCNFs powder and the PLA/PBAT composite powder were ground and pressed into pellets for FTIR analysis using a Nicolet 6700 spectrometer (Nicolet IS5, Thermo Fisher, Waltham, MA, USA). The scanning wavelength range was set from 4000 to 400 cm^{-1}. The SSCNFs/PLA/PBAT composites were characterized directly within the same wavelength range.

Transmission electron microscope (TEM)

The morphology of the SSCNFs was characterized using a high-resolution field emission transmission electron microscope (FEI Talos F200X, Thermo Fisher Scientific, USA). The SSCNFs suspension was diluted 100-fold and subjected to ultrasonication for 10 min. A drop of the diluted suspension was then deposited onto a copper grid and allowed to dry at room temperature prior to observation.

Scanning electron microscopy (SEM)

The cross-sectional morphology of the composites was observed using an SU1510 scanning electron microscope (Hitachi, Tokyo, Japan) at an accelerating voltage of 10 kV. Prior to observation, the samples were cryogenically fractured in liquid nitrogen. The fractured specimens were mounted on SEM stubs using conductive adhesive, ensuring that the fracture surface was flush with the stub. Finally, the samples were sputter-coated (Au/Pd 60/40; Heraeus, Hanau, German) with a thin layer of gold to enhance conductivity.

Ultraviolet-visible spectrum (UV)

UV test using 1 mm thick composite sheets. The optical transmittance of the composite sheet was measured using a UV-Vis spectrometer (Shimadzu Corporation, Japan). The sample was placed directly into the instrument's sample holder, and the transmittance spectrum was recorded in the wavelength range of 200 to 800 nm.

Mechanical property testing

The tensile and flexural properties of the composites were tested using an Instron 3369 universal testing machine (Norwood, MA, USA), in accordance with the GB/T 1040.2 (2006) and GB/T 9341 (2008) standards, respectively. All specimens were equilibrated at 23 °C and 50% relative humidity for 48 hours prior to testing. A beam speed of 10 mm/min was used for tensile tests and 10 mm/min for flexural tests. A minimum of five specimens were tested for each composite formulation, and the results are presented as the average value.

Thermogravimetric analysis (TGA)

The thermal stability and decomposition behavior of the composites were evaluated by thermogravimetric analysis (TGA) using a TGA Q50 instrument (TA Instruments, New Castle, DE, USA). Samples weighing approximately 5 to 10 mg were heated from room temperature to 600 °C at a constant heating rate of 10 °C/min under a nitrogen atmosphere with a flow rate of 50 mL/min.

Differential scanning calorimetry (DSC)

The DSC analysis of the composites was performed using a DSC 8000 instrument (PerkinElmer, Waltham, MA, USA) under a constant nitrogen purge. Two thermal cycles were applied to each sample (mass: 5 to 10 mg) to characterize its thermal behavior. In the first cycle, the specimen was heated from room temperature to 200 °C at a rate of 20 °C/min and held isothermally for 3 min to erase its thermal history. Subsequently, it was cooled to -10 °C at a rate of 10 °C/min to obtain the crystallization curve. Finally, a second heating cycle was performed from -10 °C to 200 °C at 10 °C/min after a 3-minute hold at the initial temperature. The characteristic temperatures of the crystallization peak (T_c) during cooling and the melting (T_m) and glass transition (T_g) peaks from the second heating scan were recorded.

Water contact angle (WCA)

The static water contact angle was measured using a dynamic contact angle analyzer (VCA Optima, AST Products, Inc., Billerica, MA, USA). A syringe was set to dispense approximately 1.5 µL of deionized water. The dynamic process of the droplet contacting the sample surface was recorded, and the contact angle was measured immediately after the droplet was deposited. Five measurements were performed for each sample, and the average value was reported.

Water absorption

The water absorption of the composites was measured according to the Chinese National Standard GB/T 1034 (2008). Both the 24-h and the saturation (equilibrium) water absorption values were determined. Including the two time points "24 hours" and "30 days" of saturated absorption.

RESULTS AND DISCUSSION

Particle Size and Zeta Potential Analysis of SSCNFs

Particle size and zeta potential are fundamental parameters for characterizing nanoparticles, as they reflect the particles, size and surface charge characteristics. The particle size of SSCNFs was measured by dynamic light scattering (DLS), while the zeta potential was determined *via* electrophoretic mobility, which quantifies the velocity of particle movement under an applied electric field.

As shown in Fig. 2a, the SSCNFs obtained through TEMPO oxidation and ultrasonication exhibited a narrow size distribution with an average hydrodynamic diameter of approximately 200 nm. Figure 2b reveals that these SSCNFs possess a strong negative surface charge, evidenced by a zeta potential of approximately -54 mV. This high absolute zeta potential value indicates excellent colloidal stability in aqueous suspension (Lichtenstein and Lavoine 2017). The strong electrostatic repulsion between the negatively charged fibers effectively prevents aggregation, resulting in a well-dispersed and stable aqueous solution.

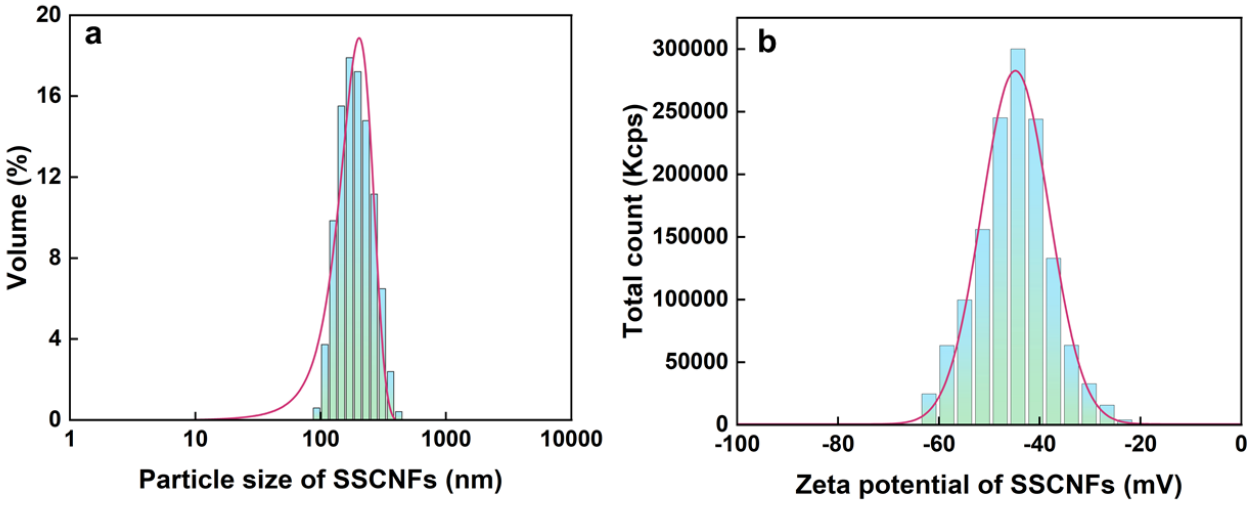

Fig. 2. Particle size distribution of SSCNFs (a) and Zeta potential distribution of SSCNFs (b)

FTIR Analysis

The FTIR analysis can effectively characterize the major functional groups and analyses the molecular interactions of SSCNFs, PLA/PBAT, and SSCNFs-PLA/PBAT composites.

Figure 3a shows the FTIR spectrum of the prepared SSCNFs. The broad peak observed at approximately 3420 cm^{-1} is attributed to the O-H stretching vibration of hydroxyl groups (Fortunati *et al*. 2016). The relatively weak peak at 2900 cm^{-1}, assigned to C-H stretching. The appearance of a distinct peak at 1610 cm^{-1}, corresponding to the carboxylate group (COO^-), confirms the successful oxidation of hydroxyl groups to carboxylates by the TEMPO-mediated reaction. This result indicates the introduction of a substantial number of carboxyl groups onto the cellulose nanofibers (Isogai and Zhou 2019).

Figure 3b demonstrates the FTIR spectra of PLA/PBAT composites prepared by co-precipitation method, 1760 cm^{-1} is the expansion vibration peak of the ester group of the PLA chain, and 3500 cm^{-1} is the expansion and contraction vibration absorption peak of the hydroxyl group of the PBAT chain. The active epoxy group of the chain extender ADR underwent a ring-opening reaction with the terminal hydroxyl group or carboxyl group of the PLA and PBAT molecular chains and the reaction was complete to obtain PLA/PBAT copolyester (Zhao *et al*. 2023), illustrating how well ADR can act as a bridge between the two to improve their compatibility.

Figure 3c displays the FTIR spectrum of the SSCNFs/PLA/PBAT composite prepared by the hot-pressing method. The spectrum shows the characteristic peaks of both SSCNFs and the PLA/PBAT copolyester. The absence of any new absorption peaks indicates that no chemical reaction occurred during the hot-pressing process, and the components are simply physically blended.

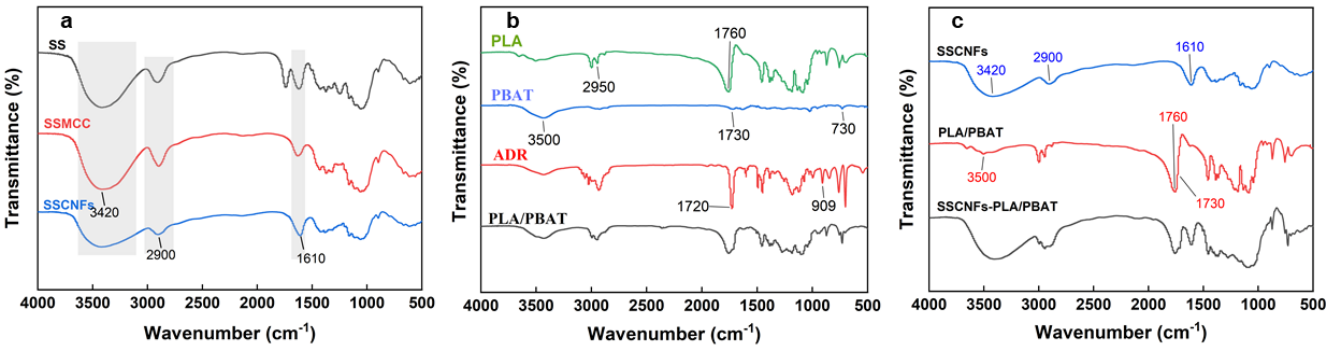

Fig. 3. FTIR spectra of SSCNFs (a), PLA/PBAT (b), and SSCNFs/PLA/PBAT (c)

TEM Analysis

The SSCNFs observed under TEM showed a typical elongated fibrillar morphology, with their diameters uniformly distributed between 3 and 20 nm and their lengths in the range of 100 to 1000 nm. These nanofibrils have smooth surfaces and homogeneous morphology and are interconnected with each other to form a loosely structured and uniformly distributed three-dimensional nanofibrillar network. (Fig. 4).

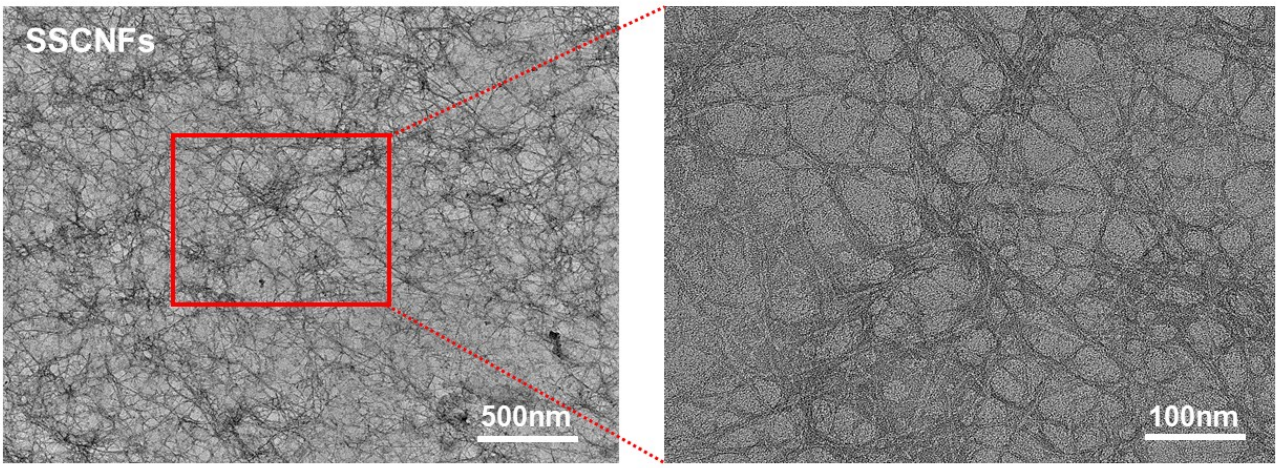

Fig. 4. TEM images of SSCNFs

SEM Analysis

Figure 5 demonstrates scanning electron micrographs of liquid nitrogen fracture of PLA/PBAT composite and SSCNFs/PLA/PBAT composite. As shown, the pure PLA/PBAT composite had a smooth cross-section and a clear and flawless texture. After the addition of SSCNFs, the cross-section became uneven. However, it can be clearly seen that SSCNFs were evenly dispersed and embedded in the composite. There was no obvious gap between the SSCNFs and the PLA/PBAT matrix, and the SSCNFs were tightly encapsulated by the PLA/PBAT matrix. In addition, the cross-section of SSCNFs/PLA/PBAT composites exhibited a porous structure, which can be attributed to the fact that SSCNFs are pulled off when brittle, forming many dimples.

The reason why SSCNFs can be well dispersed in PLA/PBAT composites and the two-phase bonding between SSCNFs and PLA/PBAT is good is attributed to the fact that there are a large number of oxygen atoms on the surface of PLA/PBAT composites, which can form hydrogen bonds with the hydroxyl groups on the surface of SSCNFs, and the effect of the hydrogen bonding makes both of them well bonded together (Hosseinnezhad *et al*. 2021). In addition, the high aspect ratio and specific surface area of SSCNFs can be physically entangled with PLA/PBAT molecular chains to enhance the interfacial bonding. During the hot-pressing process, the mobility of PLA/PBAT matrix is enhanced at high temperature, which can better infiltrate the surface of SSCNFs and form a tight interfacial bond.

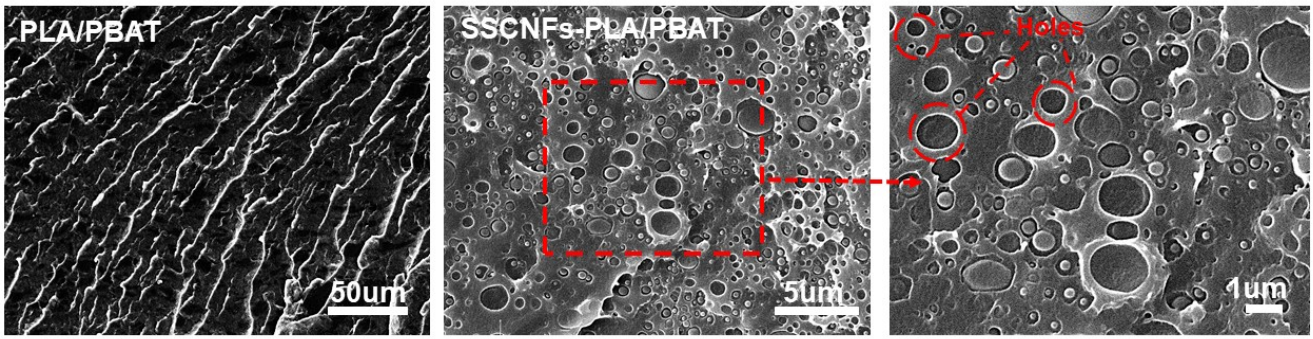

Fig. 5. SEM images of PLA/PBAT composite and SSCNFs/PLA/PBAT composite

Mechanical Property Analysis

The incorporation of SSCNFs substantially influenced the mechanical properties of the PLA/PBAT composites. The tensile and flexural properties of composites with varying SSCNFs content were evaluated using a universal testing machine (Instron 3369, Norwood, MA, USA), with the results presented in Fig. 6.

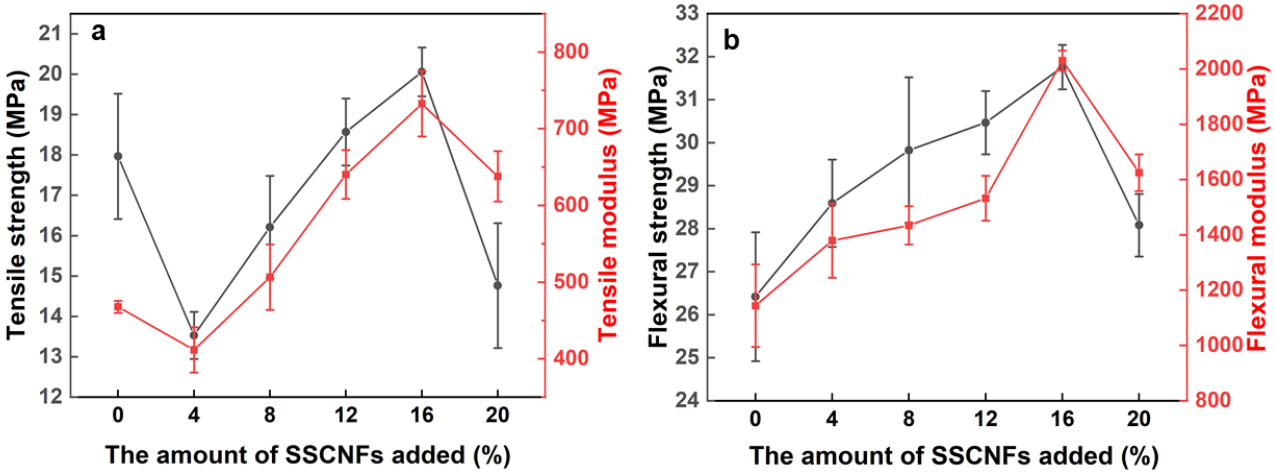

Fig. 6. The tensile properties and (a) flexural properties (b) of SSCNFs/PLA/PBAT composites

As shown in Fig. 6(a), with 4 wt% SSCNFs, the composite's tensile strength and modulus decreased relative to the pure PLA/PBAT matrix, which was possibly because the nanoparticles disrupted matrix continuity and acted as stress concentrators (Çoban *et al*. 2017). However, increasing the SSCNFs content to 8 to 16 wt% significantly enhanced these properties. The optimum was observed at 16 wt%, where the tensile strength and modulus reached 20.06 ± 0.61 MPa and 732.57 ± 42.72 MPa, respectively, corresponding to improvements of 11.7% and 56.6% over the pure matrix. This reinforcement is explained by two key mechanisms: substantial energy consumption from fiber pull-out and the development of a well-dispersed reinforcing network that transfers stress and reduces brittleness, both contributing to the improved performance *via* fiber pull-out and crack deflection (Tham *et al*. 2022; Mu *et al*. 2023).

As shown in Fig. 6(b), the flexural properties followed a trend similar to yet more sensitive than the tensile properties. While a 4 wt% SSCNFs addition caused a slight elevation, both flexural strength and modulus increased sharply at higher contents, peaking at 16 wt% with values of 31.76 ± 0.54 MPa and 2030.42 ± 36.37 MPa. This represents a 20.2% and 77.5% improvement over the matrix, respectively. The greater enhancement, especially in modulus, stems from the strong dependence of flexural properties on material stiffness. The high modulus of the SSCNFs and their nucleation effect (which boosted crystallinity, per DSC results) synergistically improved the composite's resistance to bending deformation, leading to a more dramatic increase in flexural modulus compared to tensile modulus.

However, a further increase in SSCNFs content to 20 wt% diminished the mechanical performance. This decline is likely due to the agglomeration of nanofibers, driven by their high surface energy. These agglomerates act as structural defects that induce stress concentration, promoting premature brittle failure and ultimately compromising the mechanical integrity of the composites (Shen *et al*. 2021). Consequently, 16 wt% is identified as the optimal SSCNFs loading, striking a balance between effective dispersion

and maximum reinforcement within the PLA/PBAT matrix to achieve the best overall mechanical performance.

UV Analysis

The UV-visible transmittance spectra of the PLA/PBAT composites with varying SSCNFs content are presented in Fig. 7. The incorporation of SSCNFs resulted in nearly complete shielding of light in the ultraviolet region (200 to 300 nm). Only a small fraction of light in the visible region (300 to 800 nm) was transmitted. The transmittance of the composites in both the UV and visible regions gradually decreased with increasing SSCNFs loading. This phenomenon is attributed to the UV-blocking capability of the well-dispersed SSCNF nanoparticles, which effectively absorb and scatter ultraviolet radiation (Wang *et al*. 2019). Notably, at a 16 wt% SSCNFs loading, the transmittance was reduced 46.7% compared to that of the pure PLA/PBAT composite. These results demonstrate that SSCNFs serve as an effective ultraviolet shielding agent in the PLA/PBAT matrix (Niu *et al*. 2018).

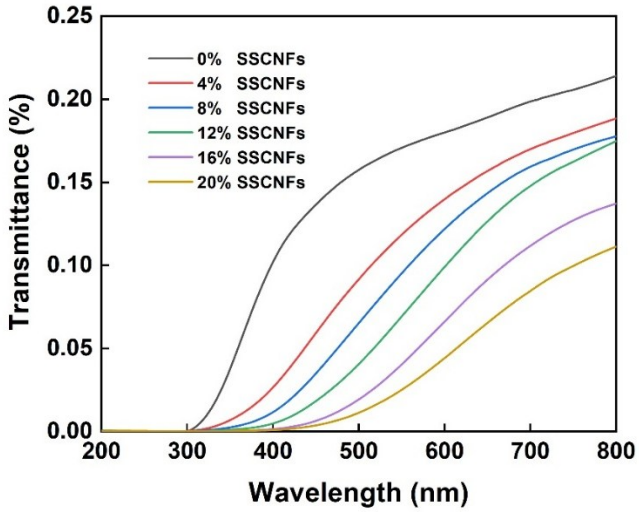

Fig. 7. UV transmittance spectra of SSCNFs/PLA/PBAT composites

Thermogravimetric Analysis

The thermal stability of the obtained SSCNFs was evaluated by TGA. As shown in the derivative thermogravimetry (DTG) curves (Fig. 8a and 8b), the SSCNFs obtained *via* TEMPO oxidation exhibited a minor mass loss event around 100 °C, which is attributed to the evaporation of bound water within the cellulose structure. The primary thermal decomposition of cellulose in the SSCNFs commenced at approximately 200 °C and was essentially complete by 400 °C. The DTG curve revealed two distinct decomposition peaks. The first peak, with a maximum at approximately 247 °C, is associated with the thermal resistance temperature of the fibers, representing the onset of major degradation. The second and more prominent peak, with a maximum at around 307 °C, corresponds to the maximum degradation rate, indicating the temperature at which the most rapid mass loss occurred.

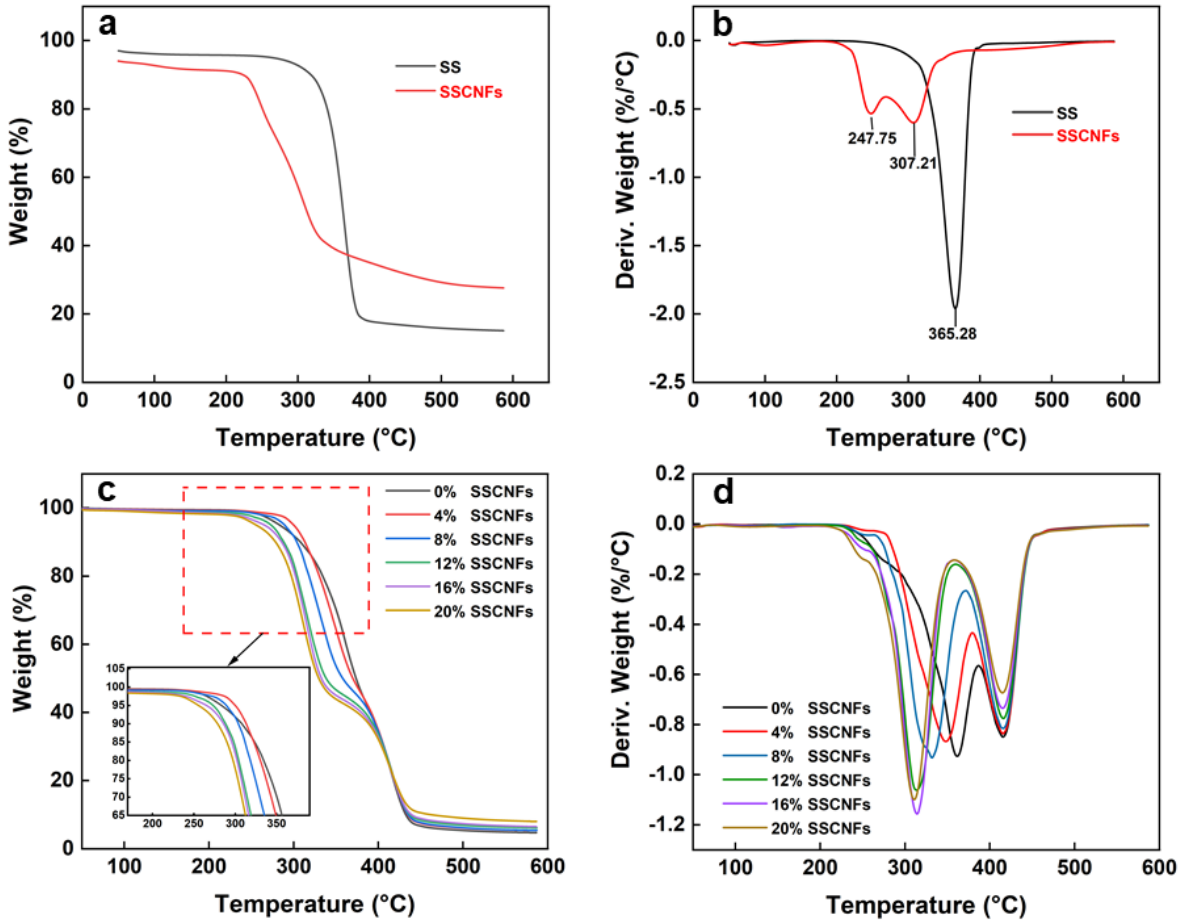

Fig. 8. TG curves (a, c) and DTG curves (b, d) of SS, SSCNFs, and SSCNFs/PLA/PBAT

The pyrolysis process of the composites, as shown in the DTG curves (Fig. 8c and 8d), primarily occurred in three distinct steps following the incorporation of SSCNFs. A minor decomposition peak observed at approximately 240 °C is attributed to the premature degradation of a portion of the SSCNFs. The principal decomposition peak of PBAT remained around 420 °C, indicating that the addition of SSCNFs did not catalyze or accelerate its thermal decomposition. However, the major decomposition peak of the composite (around 360 °C for the neat blend) shifted to a lower temperature. This downward shift suggests that the SSCNFs facilitated the decomposition of the polymer matrix, potentially by altering the degradation pathway or providing a conductive pathway for heat (D'Acierno *et al*. 2023). Furthermore, as the SSCNFs loading increased from 4 wt% to 16 wt%, the onset thermal decomposition temperature decreased from 350 to 310 °C, indicating a reduction in the overall thermal stability of the composites. This decrease in thermal stability is likely due to the nanoscale dimensions and high specific surface area of the SSCNFs. The increased surface area may enhance heat transfer and promote the earlier initiation of decomposition reactions within the polymer matrix.

Differential Scanning Calorimetry Analysis

To investigate the thermal properties of the composites with different SSCNFs additions, DSC analyses were carried out, and the DSC parameters of the SSCNFs/PLA/PBAT composites are demonstrated in Table 2.

Table 2. DSC Parameters of SSCNFs/PLA/PBAT Composites

Sample Name	T_c (°C)	T_m (°C)	T_g (°C)	ΔH_m (J/g)	χ_c (%)
0% SSCNFs	60.00	151.09	61.75	27.67	27.29
4% SSCNFs	69.34	151.66	63.24	29.80	29.39
8% SSCNFs	70.05	150.64	62.67	30.40	29.98
12% SSCNFs	70.29	150.61	62.55	30.91	30.48
16% SSCNFs	71.41	150.81	62.69	31.99	31.55
20% SSCNFs	71.02	150.87	62.77	29.03	28.63

The thermal behavior of the composites was further investigated by DSC. Figure 9a presents the cooling exotherms, while Fig. 9b shows the second heating endotherms. As shown in the cooling curves (Fig. 9a) and summarized in Table 2, the crystallization temperature (T_c) of the composites shifted to higher temperatures with the addition of SSCNFs. This shift indicates that the SSCNFs acted as effective nucleating agents, promoting crystallization and thus improving the crystallization properties of the composites (Ma *et al*. 2016). From the second heating curves (Fig. 9b), it is observed that the melting temperature (T_m) of the composites decreased slightly with increasing SSCNFs content, although this reduction was not pronounced. This marginal decrease in T_m may be attributed to potential minor degradation of the PLA matrix. The hydrolysis of the remaining hydroxyl groups on the TEMPO-oxidized cellulose nanofibers at elevated temperatures could potentially catalyze this degradation process. Furthermore, the glass transition temperature (T_g) of the composites, observed around 62 °C (the transition from a rigid glassy state to a flexible, highly elastic state), exhibited a slight increase. This suggests that the sunflower straw cellulose nanoparticles may have interacted strongly with the PLA/PBAT matrix, restricting the segmental mobility of the polymer chains at the interface.

To further quantify the effect of SSCNFs on crystallization behaviour, the crystallinity of the composites was calculated from DSC second heating data (Table 2). The crystallinity exhibited a trend of initial increase followed by a decrease with rising SSCNFs content. Specifically, it increased from 27.3% to 31.6% as the SSCNFs content rose from 0% to 16%. This trend aligns with the observed increase in crystallization temperature (T_c), collectively confirming that SSCNFs serve as an effective heterogeneous nucleating agent, promoting the orderly arrangement of PLA molecular chains and crystal formation during cooling. The rise in crystallinity is a key factor behind the notable improvement in tensile and flexural modulus, as crystalline regions act as physical cross-linking points that restrict chain mobility, thereby enhancing material rigidity. However, at excessive loading (20 wt%), nanofiber agglomeration likely impedes the full extension and rearrangement of PLA chains, leading to a retardation or slight decline in crystallinity growth. This decline in structural perfection is directly corroborated by the corresponding deterioration in mechanical properties.

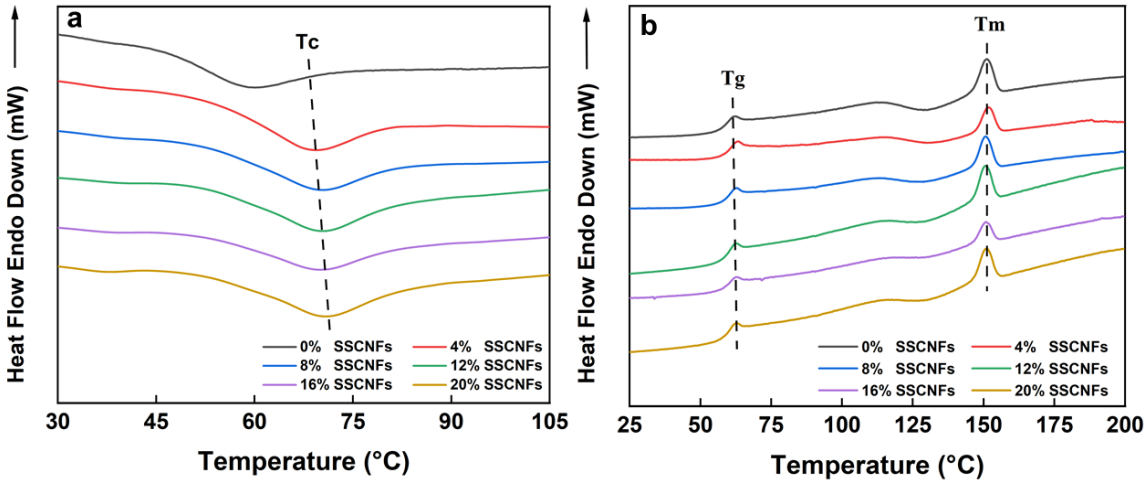

Fig. 9. The cooling (a) and heating (b) curves of SSCNFs/PLA/PBAT composites

WCA Analysis

The water contact angles of the composites with different SSCNFs loadings are presented in Fig. 10. The WCA initially increased and then decreased with increasing SSCNFs content. A maximum WCA of nearly 100° was achieved at a 16 wt% SSCNFs loading, indicating that the material exhibited slight hydrophobicity (Su and Li 2010). This increase in hydrophobicity is likely due to the incorporation of an optimal amount of SSCNFs, which altered the surface morphology and increased the roughness of the composite.

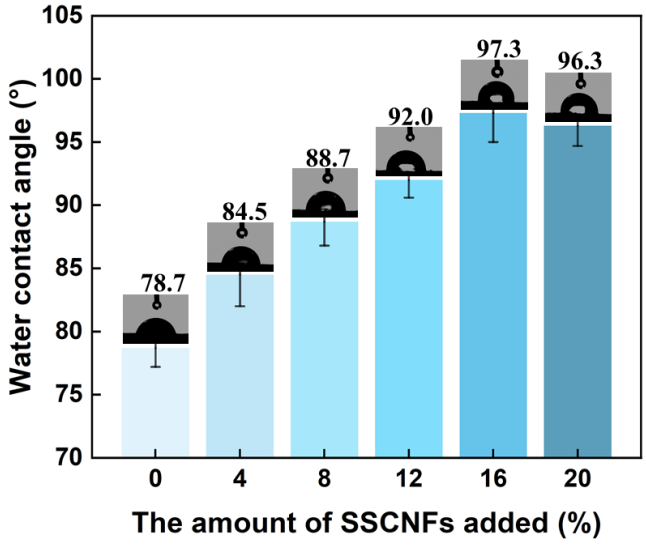

Fig. 10. Water contact angle of SSCNFs/PLA/PBAT composites

Enhanced surface roughness can lead to larger contact angles by reducing the effective contact area between the water droplet and the solid surface (Pan *et al*. 2024). Conversely, at higher SSCNFs loadings, the WCA decreased. This reduction can be attributed to the hydrophilic nature of cellulose dominating the surface properties.

Excessive SSCNFs may have created a less dense composite surface structure with higher porosity, facilitating water absorption and consequently reducing the contact angle.

Water Absorption Analysis

The water absorption behavior of the SSCNFs/PLA/PBAT composites was measured over a period of 30 days (Fig. 11). A significant uptake of water was observed within the first 24 h, which is a common phenomenon in polymer composites (Aouay *et al*. 2024). The overall water absorption rate exhibited a trend of initial increase followed by a subsequent decrease with increasing SSCNFs content.

This complex behavior can be explained by two competing mechanisms. Initially, at lower loadings, the incorporation of a small number of SSCNF nanoparticles may disrupt the original dense structure of the PLA/PBAT matrix. This disruption can create additional voids and microgaps at the interfaces, providing pathways for water ingress and leading to an increase in the water absorption rate. Conversely, at higher or optimal loadings, well-dispersed SSCNFs can effectively fill the existing pores and voids within the matrix. More importantly, they can form a continuous "network structure." This network acts as a barrier, hindering the penetration and diffusion of water molecules through the composite and thereby reducing the overall water absorption and improving the composite's resistance to water.

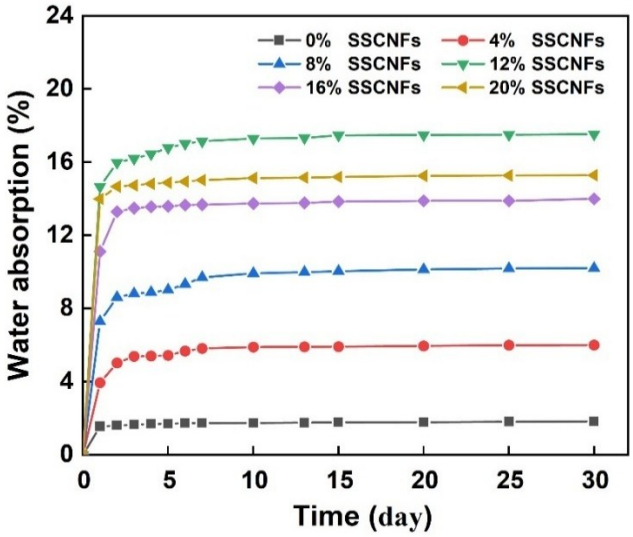

Fig. 11. Water absorption of SSCNFs/PLA/PBAT composites

CONCLUSIONS

1. This study demonstrated that a combined co-precipitation and thermo-compression moulding approach is a viable strategy for ensuring the uniform dispersion of sunflower straw cellulose nanofibers (SSCNFs) in a poly(lactic acid)/poly(butylene adipate-co-terephthalate) (PLA/PBAT) blend. The fabricated composites achieved a favorable profile of mechanical, UV-shielding, and hydrophobic properties, underscoring their potential as competitive, fully biodegradable alternatives for packaging applications.
2. The enhancement of mechanical properties achieved in this study by incorporating SSCNFs into the PLA/PBAT matrix was more pronounced than that reported by Deniz

Sema Sarul *et al.* (2021) for composites reinforced with cellulose nanocrystals (CNC). When the SSCNFs content reached 16 wt%, the mechanical properties of the composites were optimized: tensile strength increased 11.7%, tensile modulus increased 56.6%, flexural strength increased 20.2%, and flexural modulus increased 77.5%. With the increase in the content of SSCNFs, the crystalline properties of the composites were remarkably enhanced, the UV shielding ability was improved, and the hydrophobicity was enhanced. Conversely, increasing the SSCNFs loading negatively impacted the thermal stability of the composites, resulting in a gradual decrease in thermal decomposition temperatures. The experimental results demonstrate that SSCNFs are an effective reinforcing material, and a 16 wt% loading represents the optimal balance for achieving the best overall performance.

3. In this work, a series of SSCNFs/PLA/PBAT composites with varying SSCNFs ratios were developed, providing a green and feasible strategy for producing low-cost, biodegradable packaging materials. These findings indicate that SSCNFs/PLA/PBAT composites have great potential as biocomposites for food packaging applications. This approach could reduce the reliance on non-renewable plastics and help alleviate environmental pollution. It should be noted that this study did not encompass dynamic mechanical analysis (DMA) or accelerated aging experiments. Future investigations will be essential to comprehensively understand the material's long-term performance and the scalability of the fabrication process.

ACKNOWLEDGMENTS

This work was supported by the China Postdoctoral Science Foundation (No. 200902090) and Tianjin Enterprise Science and Technology Commissioner Project (No. 21YDTPJC00570).

REFERENCES CITED

Aouay, M., Magnin, A., Lancelon-Pin, C., Putaux, J. L., and Boufi, S. (2024). "Mitigating the water sensitivity of PBAT/TPS blends through the incorporation of lignin-containing cellulose nanofibrils for application in biodegradable films," *ACS Sustainable Chemistry & Engineering* 12(29) 10805-10819. https://doi.org/10.1021/acssuschemeng.4c02245

Binici, H., Aksogan, O., Dıncer, A., Luga, E., Eken, M., and Isikaltun, O. (2020). "The possibility of vermiculite, sunflower stalk and wheat stalk using for thermal insulation material production, " *Science and Engineering Progress* 18, article 100567. https://doi.org/10.1016/j.tsep.2020.100567

Çoban, O., Bora, M. Ö., Kutluk, T., and Özkoç, G. (2017). "Mechanical and thermal properties of volcanic particle filled PLA/PBAT composites," *Polymer Composites* 39(S3), E1500-E1511. https://doi.org/10.1002/pc.24393

D'Acierno, F., Michal, C. A., and MacLachlan, M. J. (2023). "Thermal stability of cellulose nanomaterials," *Chemical Reviews* 123(11), 7295-7325. https://doi.org/10.1021/acs.chemrev.2c00816

Da Costa, F. A. T., Parra, D. F., Cardoso, E. C. L., and Güven, O. (2023). "PLA, PBAT, cellulose nanocrystals (CNCs), and their blends: Biodegradation, compatibilization, and nanoparticle interactions," *Journal of Polymers and the Environment* 31(11), 4662-4690. https://doi.org/10.1007/s10924-023-02899-7

Dalmis, R. (2023). "Description of a new cellulosic natural fiber extracted from *Helianthus tuberosus L*. as a composite reinforcement material," *Physiologia Plantarum* 175(4), article e13960. https://doi.org/10.1111/ppl.13960

Deniz Sema Sarul, Arslan, D., Vatansever, E., Kahraman, Y., Durmuş, A., Reza Salehiyan, and Mohammadreza, N. (2021). "Preparation and characterization of PLA/PBAT/CNC blend nanocomposites," *Colloid and Polymer Science* 299(6), 987-998. https://doi.org/10.1007/s00396-021-04822-9

Ewulonu, C. M., Liu, X., Wu, M., and Huang, Y. (2019). "Ultrasound-assisted mild sulphuric acid ball milling preparation of lignocellulose nanofibers (LCNFs) from sunflower stalks (SFS)," *Cellulose* 26(7), 4371-4389. https://doi.org/10.1007/s10570-019-02382-4

Fortunati, E., Luzi, F., Jiménez, A., Gopakumar, D. A., Puglia, D., Thomas, S., Kenny, J. M., Chiralt, A., and Torre, L. (2016). "Revalorization of sunflower stalks as novel sources of cellulose nanofibrils and nanocrystals and their effect on wheat gluten bionanocomposite properties," *Carbohydrate Polymers* 149, 357-368. https://doi.org/10.1016/j.carbpol.2016.04.120

Hosseinnezhad, R., Vozniak, I., and Zaïri, F. (2021). "*In situ* generation of green hybrid nanofibrillar polymer-polymer composites—A novel approach to the triple shape memory polymer formation," *Polymers* 13(12), article 1900. https://doi.org/10.3390/polym13121900

Isogai, A., and Zhou, Y. (2019). "Diverse nanocelluloses prepared from TEMPO-oxidized wood cellulose fibers: Nanonetworks, nanofibers, and nanocrystals," *Current Opinion in Solid State and Materials Science* 23(2), 101-106. https://doi.org/10.1016/j.cossms.2019.01.001

Jamshidian, M., Tehrany, E. A., Imran, M., Jacquot, M., and Desobry, S. (2010). "Poly-lactic acid: Production, applications, nanocomposites, and release studies," *Comprehensive Reviews in Food Science and Food Safety* 9(5), 552-571. https://doi.org/10.1111/j.1541-4337.2010.00126.x

Lichtenstein, K., and Lavoine, N. (2017). "Toward a deeper understanding of the thermal degradation mechanism of nanocellulose," *Polymer Degradation and Stability* 146, 53-60. https://doi.org/10.1016/j.polymdegradstab.2017.09.018

Ma, P., Jiang, L., Yu, M., Dong, W., and Chen, M. (2016). "Green antibacterial nanocomposites from poly(lactide)/poly(butylene adipate-*co*-terephthalate)/ nanocrystal cellulose–silver nanohybrids," *ACS Sustainable Chemistry & Engineering* 4(12), 6417-6426. https://doi.org/10.1021/acssuschemeng.6b01106

Mu, W., Chen, X., Li, S., Sun, Y., Wang, Q., and Jingxin Na. (2023). "Mechanical performances analysis and prediction of short plant fiber-reinforced PLA composites," *Polymers* 15(15), article 3222. https://doi.org/10.3390/polym15153222

Niu, X., Liu, Y., Fang, G., Huang, C., Rojas, O. J., and Pan, H. (2018). "Highly transparent, strong, and flexible films with modified cellulose nanofiber bearing UV shielding property," *Biomacromolecules* 19(12), 4565-4575. https://doi.org/10.1021/acs.biomac.8b01252

Pan, H., Yu, T., Zheng, Y., Ma, H., Shan, J., Yi, X., Liu, Y., Zhan, J., Wang, W., and Zhou, H. (2024). "Isolation, characteristics, and poly(butylene adipate-co-

terephthalate) (PBAT) degradation mechanism of a marine bacteria *Roseibium aggregatum* ZY-1," *Marine Pollution Bulletin* 201, article 116261. https://doi.org/10.1016/j.marpolbul.2024.116261

Salzano de Luna, M., and Filippone, G. (2016). "Effects of nanoparticles on the morphology of immiscible polymer blends – Challenges and opportunities," *European Polymer Journal* 79, 198-218. https://doi.org/10.1016/j.eurpolymj.2016.02.023

Shen, J., Li, X., and Yan, X. (2021). "Mechanical and acoustic properties of jute fiber-reinforced polypropylene composites," *ACS Omega* 6(46), 31154-31160. https://doi.org/10.1021/acsomega.1c04605

Su, C., and Li, J. (2010). "The friction property of super-hydrophobic cotton textiles," *Applied Surface Science* 256(13), 4220-4225. https://doi.org/10.1016/j.apsusc.2010.02.006

Taguet, A., Cassagnau, P., and Lopez-Cuesta, J.-M. (2014). "Structuration, selective dispersion and compatibilizing effect of (nano)fillers in polymer blends," *Progress in Polymer Science* 39(8), 1526-1563. https://doi.org/10.1016/j.progpolymsci.2014.04.002

Tham, M. W., M. R., Nurul Fazita, Abdul Khalil, H. P. S., Jaafar, M., Rashedi, A., and Mohamad Haafiz, M. K. (2022). "Biocomposites based on poly(lactic acid) matrix and reinforced with natural fiber fabrics: The effect of fiber type and compatibilizer content," *Polymer Composites* 43(7), 4191-4209. https://doi.org/10.1002/pc.26681

Wang, W., Zhang, B., Jiang, S., Bai, H., and Zhang, S. (2019). "Use of CeO_2 nanoparticles to enhance UV-shielding of transparent regenerated cellulose films," *Polymers* 11(3), article 458. https://doi.org/10.3390/polym11030458

Xu, M., Qi, M., Goff, H. D., and Cui, S. W. (2020). "Polysaccharides from sunflower stalk pith: Chemical, structural and functional characterization," *Food Hydrocolloids* 100, article 105082. https://doi.org/10.1016/j.foodhyd.2019.04.053

Yan, C., Yin, Y., Zhang, S., Luo, G., Xu, Y., Liu, L., Luo, J., and Zhou, X. (2023). "Fabrication and characterization of sunflower oil-in-water emulsions stabilized with sunflower stem pith cellulose nanofibril," *International Journal of Biological Macromolecules* 224, 919-926. https://doi.org/10.1016/j.ijbiomac.2022.10.177

Yan, D., Wang, Z., Guo, Z., Ma, Y., Wang, C., Tan, H., and Zhang, Y. (2020). "Study on the properties of PLA/PBAT composite modified by nanohydroxyapatite," *Journal of Materials Research and Technology* 9(5), 11895-11904. https://doi.org/10.1016/j.jmrt.2020.08.062

Zhao, X., Yu, J., Wang, X., Huang, Z., Zhou, W., and Peng, S. (2023). "Strong synergistic toughening and compatibilization enhancement of carbon nanotubes and multi-functional epoxy compatibilizer in high toughened polylactic acid (PLA)/poly (butylene adipate-co-terephthalate) (PBAT) blends," *International Journal of Biological Macromolecules* 250, article 126204. https://doi.org/10.1016/j.ijbiomac.2023.126204

Article submitted: September 1, 2025; Peer review completed: October 5, 2025; Revised version received: November 3, 2025; Accepted: January 15, 2026; Published: February 4, 2026.
DOI: 10.15376/biores.21.2.2815-2831